Counterion Distribution around a Spherical Polyelectrolyte Brush Probed by Anomalous Small-Angle X-ray Scattering

N. Dingenouts,[†] M. Patel,[‡] S. Rosenfeldt,[‡] D. Pontoni,[§] T. Narayanan,[§] and M. Ballauff*[,‡]

Polymer-Institut, Universität Karlsruhe, Kaiserstrasse 12, 76128 Karlsruhe, Germany; Physikalische Chemie I, University of Bayreuth, 95440 Bayreuth, Germany; and ESRF, B.P. 220, 38043 Grenoble Cedex, France

Received September 10, 2003; Revised Manuscript Received August 17, 2004

ABSTRACT: We have used anomalous small-angle X-ray scattering (ASAXS) to investigate the spatial correlation of counterions with a macroion consisting of polyelectrolyte brushes. The spherical polyelectrolyte brush is composed of a solid poly(styrene) core of 68 nm radius with a dense grafting of linear poly(acrylic acid) chains and rubidium counterions. ASAXS allows one to evaluate the spatial distribution of counterions by exploiting the selective variation in contrast near the absorption edge of rubidium. The deduced spatial distribution of the counterions shows that they are closely correlated to the polymer chains of the macroion. The correlation between ions and polymer chains in these brushes is much stronger than that found in linear polyelectrolytes.

I. Introduction

If linear polyelectrolyte chains are densely affixed onto a planar or curved surface, a polyelectrolyte brush results.[1,2] The term brush specifies that the linear dimensions of the attached chains are much greater than the distance between the chains on the surface. In the case of weak polyelectrolytes such as e.g. poly(acrylic acid) (PAA), the charges along the polymer chains depend on the pH and the system is classified as an annealed brush. Grafting of strong polyelectrolyte chains to surfaces leads to quenched brushes in which the chains are charged under arbitrary conditions. Immersed in water or a polar solvent, such a brush will be swollen. The degree of swelling along the layer will result from a balance of the electrostatic repulsion that will stretch the chains and the retracting force due to the configurational elasticity of the polymer chains.[1−3] Since the electrostatic repulsion can be tuned by added salt, the degree of swelling of polyelectrolyte brushes can be varied within a wide range.

Polyelectrolyte brushes have been the subject of a large number of theoretical studies recently.[3−17] Two different regimes have been identified:[3,4] If no salt is added, the osmotic limit is reached where the osmotic pressure of the counterions leads to a strong stretching of the chains. At high concentrations of added salt, the electrostatic interaction will be strongly screened. In this limit termed salted brush, the thickness will be determined by the mutual interaction of the chains, and the overall structure found in this case will resemble the one found for uncharged systems.[1] The main predictions of theory compare favorably with the experimental data obtained from planar brushes[18−27] which seem to be rather well-understood by now.

Strongly curved polyelectrolyte brushes, however, are much less understood. These systems can be generated by attaching polyelectrolyte chains to colloidal particles of radius R. Figure 1 displays schematically such a particle that consists of a solid polymer core and a shell of densely grafted polyelectrolyte chains. In the following these systems will be termed spherical polyelectrolyte brushes. If R exceeds the contour length L_c of the chains by far, the planar limit is recovered. If, on the other hand, $R \ll L_c$, such a spherical polyelectrolyte will resemble charged star polymers.[14,15] Spherical polyelectrolyte brushes have been prepared by adsorption of block copolymers on the surface of latex particles[28−30] and by formation of micelles from suitable block copolymers.[31−35] The latter systems have recently been the subject of detailed studies employing neutron scattering by van der Maarel and co-workers.[36−38] More recently, Förster et al. combined SANS, electron microscopy, and dynamic light scattering of micelles having a corona of polyelectrolyte chains.[35]

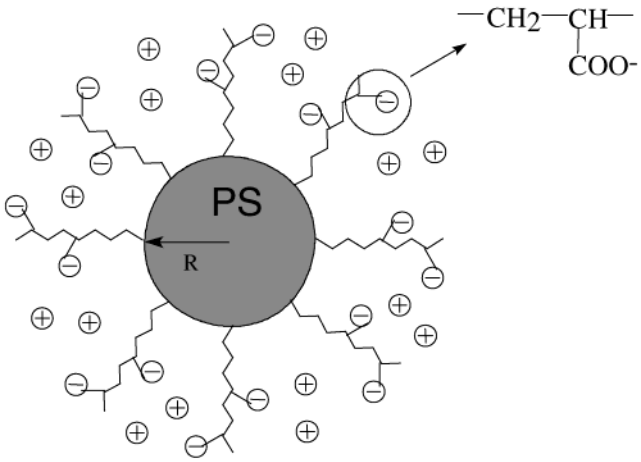

Figure 1. Scheme of the spherical polyelectrolyte brushes analyzed in this study. The particles consist of a poly(styrene) core of ca. 100 nm diameter. Onto this core linear poly(acrylic acid) (PAA) chains are grafted chemically. The distance between the chains on the surface of the core particle is much smaller than the linear dimensions of the PAA chains. Hence, the PAA chains form a brush in which the Rb^+ counterions are confined.

[†] Universität Karlsruhe.
[‡] University of Bayreuth.
[§] ESRF.
* Corresponding author. E-mail: Matthias.Ballauff@uni-bayreuth.de.

10.1021/ma048828j CCC: $27.50
Published on Web 09/24/2004

A central problem in the understanding of spherical polyelectrolyte brushes is the correlation of the counterions to the macroion. Recently, this problem has been studied theoretically for the case of polyelectrolyte stars by Jusufi, Likos, and Löwen.[39,40] In the course of this work it has been shown that the counterions can be subdivided into three classes: (i) counterions condensed to the polyelectrolyte chains because of their strong electric charge ("Manning condensation");[41,42] (ii) counterions that are trapped within the brush but can move freely there, and (iii) counterions that may leave the brush. Only the last fraction will lead to a measurable osmotic pressure. Very recently, this work has been extended to include the spherical polyelectrolyte brushes under consideration here.[43]

Spherical polyelectrolyte brushes (see Figure 1) prepared by photoemulsion polymerization[44,45] present a nearly ideal model system to check these predictions. PAA chains are grafted densely on a monodisperse solid poly(styrene) core having a diameter between 80 and 120 nm. The chains have been generated directly on the surface of the core particles by the photoinitiated radical polymerization of the water-soluble monomer acrylic acid.[44] The contour length L_c as well as the grafting density σ can be determined.[44,45] Up to now, these systems have been studied comprehensively by dynamic light scattering in highly diluted aqueous solutions as a function of pH and salinity[45,46] and by SAXS.[47] Dynamic light scattering gives the overall dimensions of the particles but gives no information on the location of the counterions. Osmometry of salt-free suspensions of the spherical polyelectrolyte brushes[48] shows that the concentration of free counterions is of the order of a few percent only. Hence, the counterions are trapped within the brush to a large extent as predicted by Jusufi, Likos, and Löwen.[39,40] No systematic experimental investigation related to these predictions is available so far.

Here we present an experimental study of the counterions within the spherical polyelectrolyte brush by anomalous small-angle X-ray scattering (ASAXS).[49−52] ASAXS combines the conventional small-angle X-ray experiment with the effect of anomalous dispersion, i.e., the change of the scattering power of an element if the energy of the incident radiation is near an absorption edge of that element. Hence, the scattering factor f_{ion} becomes a complex function of the energy E of the incident radiation near the absorption edge of the ions:[50,51]

$$f_{ion} = f_0 + f'(E) + \tilde{\imath} f''(E) \qquad (1)$$

The first term f_0 is the nonresonant term which equals the atomic number of the element.[62] The second and third terms in eq 1 are the real and the imaginary part due to the anomalous dispersion near the absorption edge, and $\tilde{\imath}$ is the complex unit. The imaginary part $f''(E)$ is directly related to the absorption cross section for X-rays of energy E. Small-angle X-ray scattering measurements near the absorption edge of the rubidium counterions allow one to change the scattering contribution of the Rb^+ ions in a systematic fashion while keeping all other contributions constant. Figure 2 displays the variation of $f'(E)$ and of $f''(E)$ calculated for rubidium. Hence, ASAXS can separately assess the spatial distribution of the macroion and the counterions which is not possible with the conventional SAXS experiment.

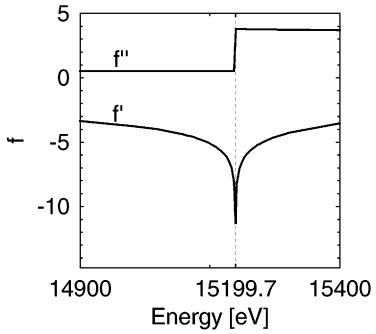

Figure 2. Dispersion of rubidium near the K-edge: the real and imaginary parts f' and f'' as a function of the energy E of the incident radiation. The vertical dashed line marks the energy of the K_α-edge of rubidium.

Up to now, ASAXS has mainly been applied to solid specimens of inorganic systems involving catalysts and metals, the absorption edge of which could easily be reached.[53−55] However, this method has hardly been used to study polyelectrolytes despite the fact that pioneering studies by Stuhrmann[50] and by Williams[52] demonstrated the power of this method when applied to charged systems. The problems of ASAXS laid in technical problems which are due to the rather small weight fraction of the anomalous scattering entities in polyelectrolyte solutions.

Very recently, we[56−58] and others[59,60] demonstrated that the high brilliance of modern synchrotron radiation sources makes an ASAXS experiment feasible for charged polymers. In particular, it has been demonstrated for the first time that all the three terms predicted a long time ago[50,52] could be obtained with good accuracy.[58,60] The Fourier transform of the cloud of counterions around a rodlike macroion could be measured directly accurately and evaluated.[58] A recent investigation of spherical polyelectrolyte brushes has demonstrated that these systems should be good candidates for an ASAXS study as well.[61] In this work, however, no systematic evaluation of the data was done.

The present study is organized as follows: We first discuss the general theory of ASAXS as applied to spherical polyelectrolyte brushes. Special emphasis will be given to the information to be deduced. Here the magnitude of the effect of ASAXS will be discussed by the help of model calculations. Then experimental determination of the ASAXS intensities and possible sources of error are discussed. Finally, the results of ASAXS measurements are presented and discussed. We shall demonstrate that the full information, i.e., all three terms,[58] can be obtained for spherical polyelectrolyte brushes as well.

II. Theory

A. ASAXS. The system investigated here consists of a dilute solution of the spherical polyelectrolyte brushes depicted schematically in Figure 1. The PAA chains affixed to the surface are fully dissociated and the negative charge of each group is balanced by a Rb^+ counterion. The energy of the incident radiation was changed to reach the absorption edge of rubidium (15 199.7 eV) from below. Near the absorption edge the scattering length of the counterion becomes a complex function.[50,51] The macroion is made up from polymers that exhibit no anomalous dispersion in the energy range used here.

The absolute scattering intensity $I(q)$ is given by[62]

$$I(q) = \frac{N}{V} I_0(q)\, S(q) \tag{2}$$

where N/V is the number of dissolved particles per volume, $I_0(q)$ is the scattering intensity of a single particle, and $S(q)$ is the structure factor. Since we work in the dilute regime, the influence of $S(q)$ is restricted to the region of smallest angles.[49] Hence, in the following $S(q) = 1$, which corresponds to a system of noninteracting particles.

Despite the spherical symmetry, the scattering intensity $I_0(q)$ is a complex quantity because the scattering factor of the Rb^+ ions has a nonvanishing imaginary part (see eq 1).[50,51] Therefore

$$I_0(q) = F(q)\, F^*(q) \tag{3}$$

where $F(q)$ is the scattering amplitude of a single particle. Because of the spherical symmetry of the particles, $F(q)$ follows as[49,62]

$$F(q) = 4\pi \int_0^\infty [\rho(r) - \rho_m] \frac{\sin qr}{qr}\, r^2\, dr \tag{4}$$

where $\rho(r)$ is the radial electron density of the spherical polyelectrolyte brush and ρ_m is the electron density of the surrounding medium water. The excess electron density $\rho(r) - \rho_m$ consists of two parts: (i) the contribution of the macroion and (ii) the contribution of the counterions which is complex.

Contrast of Macroion. The macroion is composed of a poly(styrene) core having an excess electron density $\Delta\rho_{core}$. This contrast of poly(styrene) in water is small (see ref 49 and further citations given there), and the main contributions stem from the PAA chains attached to the surface. With the radial excess electron density of the PAA chains given by $\Delta\rho_{PAA}(r)$, we have for the radial excess electron density of the macroion

$$\Delta\rho_{macroion}(r) = \Delta\rho_{core}; \quad r \le R_c$$
$$\Delta\rho_{macroion}(r) = \Delta\rho_{PAA}(r); \quad r > R_c \tag{5}$$

where R_c is the radius of the core.

Complex Contrast of Counterions. As already discussed above in conjunction with eq 1, the scattering factor f_{ion} becomes complex in the vicinity of the absorption edge. Both $f'(E)$ and $f''(E)$ are related to each other by the Kramers−Kronig relation.[50,51] Figure 2 displays the variation of f' and of f''. It is interesting to note that the imaginary part f'' remains practically constant below the edge, whereas f' shows a strong variation near the edge. Hence, the ASAXS effect will be mainly determined by the real part f' if the experiments are conducted at energies below the absorption edge. Measurements above the edge, on the other hand, would lead to strong fluorescence which may cause a high background. A previous analysis of rodlike polyelectrolytes, however, has demonstrated that measurements can be done above the edge if the background by fluorescence is subtracted properly.[58] Figure 2 also demonstrates that measurements need to be done very close to the absorption edge if a sufficient decrease of f' is to be realized.

For ions immersed in a medium with electron density ρ_m the number of excess electrons per ion Δf_{ion} follows as[56−58]

$$\Delta f_{ion} = f_0 - \rho_m V_{ion} + f'(E) + \tilde{\imath} f''(E)$$
$$= \Delta f_0 + f'(E) + \tilde{\imath} f''(E) \tag{6}$$

where V_{ion} is the volume of a single ion. The quantity Δf_0 hence denotes the scattering contribution of a single counterion that is independent of the energy of the incident radiation.

Let $n_{ion}(r)$ be the number of counterions per unit volume within distance r from the center of the particle. Then the contribution of the counterions to the excess electron density of the entire particles is given by

$$\Delta\rho_{ion}(r) = n_{ion}(r)\Delta f_{ion}; \quad r \ge R_c \tag{7}$$

From these conditions it follows that the excess electron density of the spherical polyelectrolyte brush is given by

$$\Delta\rho(r) = \Delta\rho_{core}(r); \quad r \le R_c$$
$$\Delta\rho(r) = \Delta\rho_{PAA}(r) + \Delta f_{ion}; \quad r > R_c \tag{8}$$

Calculation of $I_0(q)$ and of $v(q)$. The scattering amplitude $F(q)$ is split into a nonresonant term $F_0(q)$ and an energy-dependent term $F_{res}(q)$:

$$F(q) = F_0(q) + F_{res}(q) \tag{9}$$

For the nonresonant term we obtain from eq 5

$$F_0(q) = 4\pi \int_0^\infty \Delta\rho_{macroion} \frac{\sin qr}{qr}\, r^2\, dr + \Delta f_0 4\pi \int_{R_c}^\infty n_{ion}(r) \frac{\sin qr}{qr}\, r^2\, dr \tag{10}$$

The resonant term follows as

$$F_{res}(q) = (f'(E) + \tilde{\imath} f''(E)) 4\pi \int_{R_c}^\infty n_{ion}(r) \frac{\sin qr}{qr}\, r^2\, dr$$
$$= (f'(E) + \tilde{\imath} f''(E)) v(q) \tag{11}$$

where $v(q)$ is the Fourier transform of the distribution function of the counterions $n_{ion}(r)$. Equation 3 then leads to

$$I_0(q) = {F_0}^2(q) + 2f' F_0(q) v(q) + (f'(E)^2 + f''(E)^2 v^2(q) \tag{12}$$

Equation 12 shows that the intensity measured near the absorption edge consists of three parts: The term ${F_0}^2(q)$ denotes the nonresonant intensity that is measured far away from the edge by the conventional SAXS experiment. The second term is the cross-term of the nonresonant and the resonant amplitudes of the macroion and the counterions. It scales linearly with f' and presents in most cases the leading part of the ASAXS effect.[50] It should be kept in mind that the amplitude $F_0(q)$ embodied in this term is still related to the entire scattering object, i.e., to the spatial distribution of the nonresonant scatterers as well. Only the third term is solely related to the spatial distribution of resonantly scattering parts of the object under consideration. Its

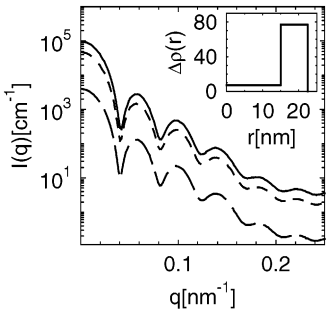

Figure 3. Model calculation: the three partial intensities obtained by an ASAXS experiment according to eq 12 are calculated for a spherical polyelectrolyte brush. The weight concentration assumed in this calculation was 6.5%. The parameters are $\Delta E = -3.1$ eV, $f' = -8.01$, and $f'' = 0.51$. The solid line denotes the intensity $I_0(q)$ measured at this energy. The short-dashed lines display the negative cross-amplitude $-2f'F_0(q)\nu(q)$ (see eq 12), whereas the long-dashed line shows the third term of eq 12.

prefactor is much smaller, however, and its measurement is concomitantly more difficult.[58]

B. Model Calculation. In the following we discuss a model calculation done for typical parameters. Hence, slightly polydisperse, concentric core−shell particle are considered. We assume system of noninteracting particles with a core diameter of 120 nm and a homogeneous shell of a thickness of 30 nm. The shell is assumed to consist of 14 wt % PAA. The contrast of the repeating unit of PAA was estimated from density data and is given by $15e^-$/unit. From this number of Rb^+ counterions confined in the shell was assumed to be the same as the number of repeating units. For the sake of simplicity we assume that the counterions are evenly distributed. The contrast of the rubidium ions is $\Delta f_{ion} = 31.5e^-/\text{nm}^3$. The latter value has been calculated from the Pauling radius of the rubidium ion (0.148 nm; see ref 63). For $\Delta\rho_{core}$ the value for poly(styrene) ($7e^-/\text{nm}^3$, calculated from density data according to ref 64) was used. To ensure a meaningful comparison with experimental scattering curves, a Gaussian size distribution with a width of 7% was used.

Figure 3 displays the result of a model calculation done for an energy of −3.1 eV according to eq 12. The different contributions to the overall intensity $I_0(q)$ are plotted as a function of the magnitude q of the scattering vector. The respective scattering factors $f' = -8.01$ and $f'' = 0.51$ are taken from the tabulations of Henke et al.[65] and of Brennan and Cowan[66] (see Table 1). Figure 3 demonstrates that the cross-term $f'F_0(q)\nu(q)$ (second term of eq 12) is of considerable magnitude in the immediate vicinity of the edge. As a consequence of this, the negative cross-term that increases linearly with f' will lead to a systematic lowering of the measured scattering curves when approaching the absorption edge. The self-term (long-dashed line in Figure 3) is smaller but presents a notable contribution to the measured intensity. All terms exhibit the same oscillations.

III. Experimental Section

A. Materials. The particles used in this study is the system L22 of ref 46 which was prepared according to refs 44 and 45 using acrylic acid as monomer. The latex was purified by extensive ultrafiltration to remove the free polymer in the serum. The characterization with regard to the contour length L_c and the grafting density was done as described in ref 46. The particles studied here had a core diameter of 68 nm, a weight-average contour length $L_c = 233$ nm, and a grafting density $\sigma = 0.026$ nm^{-2} (cf. Table 2 of ref 46).

Table 1. Scattering Factors f' and f'' (Eq 1)

ΔE[a]	f'[b]	f'_{eff}[c]	f''[d]	f''_{eff}[e]
−2737.1	−1.41	−1.41	0.74	0.74
−397.1	−3.08	−3.08	0.54	0.54
−197.1	−3.75	−3.75	0.53	0.53
−97.1	−4.44	−4.44	0.52	0.52
−47.1	−5.17	−5.17	0.52	0.52
−27.1	−5.73	−5.73	0.51	0.51
−17.1	−6.20	−6.21	0.51	0.51
−13.1	−6.47	−6.49	0.51	0.51
−9.1	−6.87	−6.88	0.51	0.51
−7.1	−7.15	−7.18	0.51	0.51
−5.1	−7.58	−7.60	0.51	0.53
−3.1	−8.01	−8.34	0.51	0.88
−1.1	−10.06	−9.69	0.51	2.23

[a] Difference of the energy of the incident beam to the absorption edge in eV. [b] Real part of the scattering factor f; see eq 1. [c] Effective real part of the scattering factor f; see text for further explanation. [d] Imaginary part of the scattering factor f; see eq 1. [e] Effective imaginary part of the scattering factor f; see text for further explanation.

The Rb^+ counterions were introduced by titration of the acidic particles by aqueous RbOH. Previous studies have shown that all carboxyl groups within the brush are converted by this procedure.[45,46] No additional salt was added to the system studied here. RbOH was added until a pH of 10 was reached. This ensured full ionization of the brush.[46]

B. ASAXS Measurements and Treatment of Data. *1. Measurements.* All ASAXS experiments reported here were carried out at the ID02A beamline of the ESRF in Grenoble, France.[67] Two sample-to-detector distances were used (2 and 10 m). The detector was an image-intensified CCD camera. The energy of the incident beam was varied between 12 460 and 15 200 eV. All data have been corrected for detector response, efficiency, and incident flux and normalized to an absolute scale. The normalized data were azimuthally averaged and corrected for the background of the water solvent and the empty cell. The data obtained at the 2 m position were deconvoluted to correct for the smearing because of the finite beam profile.[68] No desmearing was necessary for the data obtained at the 10 m position of the detector.

In situ measurement of the extinction as a function of energy was done for each sample studied here. The particle concentration was 6% to minimize the effect of particle interaction. Previous investigation had demonstrated that this concentration is low enough to disregard the influence of mutual interaction of the particles in the q range analyzed here (see ref 49 and further citations given there).

2. Correction for Fluorescence. A possible effect of fluorescence had to be taken into account in the immediate vicinity of the absorption edge because of the finite width of the energy distribution of the primary beam (see below).[58,61] The magnitude of a possible background due to fluorescence was checked through measurements at the highest scattering angles possible shown in Figure 4; $q = 3.8-4$ nm^{-1}). In the region all the scattering contributions due to structural features have decayed in very good approximation. The remaining intensity must therefore be assigned to fluorescence because all other background scattering has already been removed by subtracting the scattering of the capillary and the solvent.

The procedure is as follows: $I(q)$ obtained for $E = 15\,100$ eV (solid line in Figure 4) is assumed to be free of any background caused by fluorescence because of the sufficient resolution of the monochromator. As demonstrated by Figure 4, measurements nearer to the edge exhibited higher values of $I(q)$. This increase is solely due to fluorescence. Therefore, it is independent of q and provides a good estimate of this part of parasitic scattering. The data obtained at a given energy E are then corrected by subtracted the difference $I(q \approx 4, E) - I(q \approx 4, 15100)$ from the respective data.

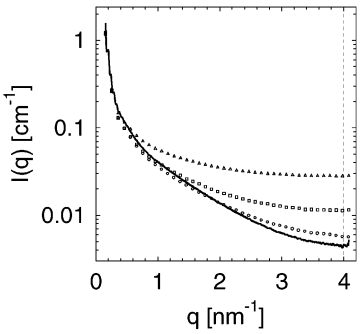

Figure 4. Correction for fluorescence. The scattering intensity $I(q)$ measured for different energies E of the incident radiation is plotted as the function of q. The solid line refers to E = 15 100 eV (ΔE = −97.1 eV) where contributions of the fluorescence can be neglected. Circles: 15 192 eV (ΔE = −5.1 eV); open squares: 15 196 eV (ΔE = −1.1 eV; triangles: 15 200 eV (ΔE = +0.3 eV).

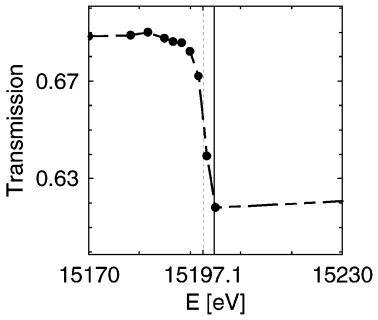

Figure 5. Determination of the position of the absorption edge.[58,61] The extinction of a typical sample is plotted against the energy of the incident beam. The solid line marks the theoretical position of the edge whereas the dotted line gives the point of inflection of the experimental transmission curve. See text for further explanation.

The correction thus effected is rather small inasmuch as the present investigation is restricted to the q range given by q < 0.6 nm^{-1}. Moreover, all data discussed here have been taken below the edge in order to minimize the problem of fluorescence. Figure 4 shows that this problem becomes appreciable only in the immediate neighborhood of the edge.

3. Localization of the Edge. Special care has been taken to localize exactly the energy of edge by careful measurements of the absorption of each sample.[58,61] Figure 5 displays as a typical example the transmission of a given solution as a function of the energy of the incident beam. The solid line marks the theoretical value of the energy of the edge (15 199.7 eV), whereas the broken line shows the point of inflection of the absorption curve. This shows that there is a small shift of the energy due to the backlash of the monochromator. This small shift was taken into account for the determination of the true energy of the incident beam. This procedure was done for each sample measured in the course of this study.

4. Effective Scattering Factors f'_{eff} and f''_{eff}. As discussed in detail previously, there is a finite width of the primary beam and the range of energies probed by a given position of the monochromator is not infinitely small.[58,61] We correct for this effect by defining the effective scattering factors f'_{eff} and f''_{eff}.[58,61] For a given energy E the respective data $f'(E)$ and $f''(E)$ are added up weighed by the energy profile of the beam. Table 1 summarized all data obtained by this procedure. In this way a small but significant correction is effected if E is in the immediate vicinity of the edge. For larger distances this correction is negligible as can be seen from Table 1. In the following, the effective quantities f'_{eff} and f''_{eff} will solely be used.

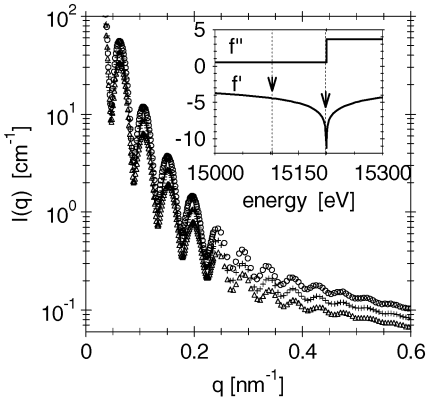

Figure 6. Dependence of the measured scattering intensity on the energy of the incident beam. The scattering intensity has been measured at 13 different energies below the edge. For the sake of clarity only three sets of data are displayed, corresponding to the difference ΔE to the absorption edge: circles, −2737. eV; crosses, −97.1 eV; triangles, −1.1 eV. The inset shows the dispersion of rubidium near the K-edge. The real and imaginary parts f' and f'' are plotted as a function of the energy E of the incident radiation.[65,66] The arrows mark the two energies of the incident radiation that correspond to the two scattering curves measured at ΔE = −97.1 and −1.1 eV, respectively.

IV. Results and Discussion

All ASAXS experiments discussed here are done using spherical polyelectrolyte brushes L22 synthesized and characterized recently.[46] These particles present annealed brushes, and the titration curves of refs 45 and 46 demonstrate that a pH of 10 is sufficient to arrive at a fully charged system. Hence, the ASAXS experiments to be discussed here are done at pH = 10. The suspensions of fully charged spherical polyelectrolyte brushes were prepared by titration of a suspension containing 6.5 wt % of the particles in water by an aqueous solution of RbOH. In this way all Rb^+ ions introduced into the system are counterions of the PAA chains, and no further salt is added. Therefore, the fully charged system may be treated as a quenched brush, and all effects due to charge annealing may be disregarded.

The ASAXS data obtained with this suspension can now be evaluated to yield the information on the distribution of the counterions around the macroion. A previous analysis had only extracted the cross-term (second term of eq 12).[61] Here we give the full analysis of the ASAXS data developed recently for the investigation of rodlike polyelectrolytes.[58]

Equation 12 shows that the intensity measured near the absorption edge consists of three parts: The term $F_0^2(q)$ denotes the nonresonant intensity that is measured far from the edge by the conventional SAXS experiment. The second term is the cross-term of the nonresonant and the resonant amplitude of the object. The third term is solely related to the spatial distribution of the counterions. Figure 6 shows that the measured scattering intensity decreases upon approaching the K-edge of the rubidium counterions. This is due to the cross-term $f'F_0(q)v(q)$ in eq 12 that is negative because of the sign of f' (see Figure 2). Figure 6 demonstrates that the shift of the scattering curves is a robust effect that can be measured without major problems if precise absolute intensities are available.

The model calculations displayed in Figure 3 have shown that the strong effect seen in Figure 6 should be expected for the present system. Hence, the third term

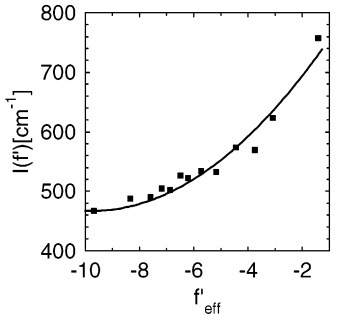

Figure 7. Dependence of $I(q)$ on the real part f' according to eq 12 for $q = 0.0265$ nm^{-1}. The solid line shows the fit of eq 12 with neglect of f''_{eff} (see also ref 58). This procedure is repeated for all q values in order to obtain the three partial intensities displayed in Figure 8.

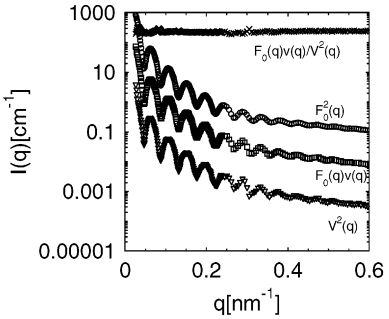

Figure 8. Decomposition of the measured ASAXS intensity $I_0(q)$ according to eq 12. All terms have been obtained from linear regression. The upper curve displays the ratio of the second and the third term of eq 13.

in eq 12 is expected to be nonnegligible as well. All data have been taken below the edge where f'' is small. Hence, the procedure suggested recently[58] for the decomposition of the data can be applied without restriction: f''_{eff} is small except at the last point below the edge (see Table 1), and therefore $f''^2_{eff} \ll f'^2_{eff}$. Therefore, $I(q)$ for a given value of q becomes a quadratic form in f'_{eff} in a very good approximation. All terms can be determined from experimental data by a linear regression. Figure 7 shows the respective plot, i.e., $I(q)$ as the function of f'_{eff}. For the sake of clarity only one set of data for a single value of q is shown. Note that 13 different energies have been used to generate this plot. The finite curvature demonstrates that the third term of eq 12 having f'^2_{eff} as a prefactor is nonnegligible. The solid line shows the fit of eq 12 for $q = 0.0265$ nm^{-1}. All terms enumerated in eq 12 can be obtained by repeating this procedure for all q values under consideration. Figure 7 demonstrates at the same time that measurements far below the absorption edge are as important as data points in the immediate neighborhood of the edge. The secure determination of all the three partial intensities rests on a precise analysis of the curvature of this plot. The range of f' covered by this analysis must therefore be wide enough.

Figure 8 displays all three terms enumerated in eq 12. It demonstrates that the entire information embodied in ASAXS measurements can be determined with good accuracy from experimental data despite the fact that the third term is small. Similar to the case of rodlike polyelectrolytes,[58] all terms in eq 12 have been obtained.

The result shown in Figure 3 can now be used to test the prediction of Jusufi et al.[39,40] in a qualitative manner. Equations 12 and 10 suggests to plot the

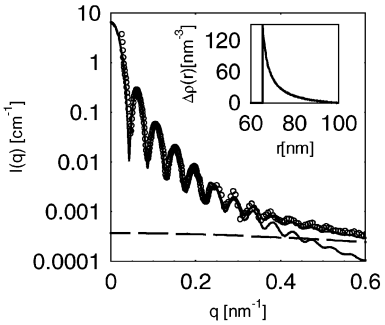

Figure 9. Partial scattering intensity of the counterions $v^2(q)$ as the function of q (see eq 12). The solid lines represent the fit by the radial profile of the excess electron density displayed in the inset. The dashed line displays the Lorentzian term due to fluctuations of the PE chains grafted to the surface of the core particles.

second term $F_0(q)v(q)$ divided by the third term $v^2(q)$ as a function of q:

$$\frac{F_0(q)\, v(q)}{v^2(q)} = \frac{F_M(q)}{v(q)} + \Delta f_0 \qquad (13)$$

Hence, ASAXS allows one to obtain the ratio of $F_M(q)$, the Fourier transform of the radial distribution of the macroions, and $v(q)$, the Fourier transform of the counterion distribution. The crosses in Figure 8 show that this ratio is a constant except for the region of smallest scattering angles. This demonstrates directly that both distributions have the same dependence on the radial distance r. The reason for this finding is the strong correlation of the counterions to the polyelectrolyte chains grafted to the surface of the core particles as predicted by Jusufi et al.[39,40]

As shown by Figure 8, ASAXS leads directly to $v^2(q)$, which is the scattering intensity of the cloud of counterions. This term can be evaluated to yield the radial distribution of the counterions $n(r)$. This analysis is shown in Figure 9. The term $v^2(q)$ (see Figure 8) has been fitted by a radial profile that assumes highly stretched chains; i.e., the distribution $n(r)$ should scale as r^{-2}. The chains grafted to the surface, however, have been generated by a radical polymerization and are therefore polydisperse.[45] This effect may be taken care by assuming an average profile as shown in the inset of Figure 9. As seen in a previous study, there is an additional scattering contribution that is due to the fluctuations of the polymer chains and the counterions at the surface.[47] This contribution that hardly comes into play in the present q range may be described by a Lorentzian:

$$I_{fluct}(q) = I_{fluct}(0)/(1 + q^2\xi^2) \qquad (14)$$

Its contribution is shown by a dashed line in Figure 9. It becomes important only for scattering angles for which $q > 0.4$ nm^{-1}.

The good agreement between theory and experiment seen in Figure 9 shows that the polyelectrolyte chains are stretched as predicted by the theory.[39,40] It should be noted that the determination of the profile can be done very accurately given the fact that 8−10 side maxima are seen in all scattering curves. Moreover, the spatial resolution of the experiment expressed in the product of the maximum q value and the core radius of the particles is ca. 40. Hence, the present experiment

already looks into the fine details of the brush layer attached to the surface of the cores. In this way the results obtained from these ASAXS experiments can directly be compared to data obtained from reflectivity measurements on planar systems.[22,24,26]

V. Conclusion

We have presented the first complete analysis of a colloidal PE brush by ASAXS. We have demonstrated the strong correlation of the counterions to the grafted polyelectrolyte chains. ASAXS leads to precise analysis of the distribution of the counterions around macroions for conventional ions such as Rb^+, thus obviating the need for labeled systems. Hence, the analysis via ASAXS as presented here leads to the investigation of subtle effects related to PE. The data presented here demonstrate that the counterions are strongly correlated with the macroion in accord with theory.[39,40] The technique presented here also has a great potential for the investigation of the effective interactions between PE brushes in concentrated solutions.[39,40]

Acknowledgment. Financial support by the Deutsche Forschungsgemeinschaft, by the Center of Functional Nanostructures (cfn of the University of Karlsruhe), the ESRF for allocation of beamtime, and by the European Community, Project HUSC, is acknowledged.

References and Notes

(1) Fleer, G. M.; Cohen Stuart, M. A.; Scheutjens, J. M. H. M.; Cosgrove, T.; Vincent, B. *Polymers at Interfaces*; Chapman and Hall: London, 1993.
(2) Dubreuil, F.; Guenon, P. *Eur. Phys. J.* **2001**, *5*, 59.
(3) Pincus, P. *Macromolecules* **1991**, *24*, 2912.
(4) Borisov, O. V.; Birshtein, T. M.; Zhulina, E. B. *J. Phys. II* **1991**, *1*, 521.
(5) Zhulina, E. B.; Borisov, O. V.; Birshtein, T. M. *J. Phys. II* **1992**, *2*, 63.
(6) Argiller, J. F.; Tirrell, M. *Theor. Chim. Acta* **1992**, *82*, 343.
(7) Borisov, O. V.; Zhulina, E. B.; Birshtein, T. M. *Macromolecules* **1994**, *27*, 4795.
(8) Zhulina, E. B.; Birshtein, T. M.; Borisov, O. V. *Macromolecules* **1995**, *28*, 1491.
(9) von Goeler, F.; Muthukumar, M. *Macromolecules* **1995**, *28*, 6608.
(10) Lyatskaya, Yu. V.; Leermakers, F. A. M.; Fleer, G. J.; Zhulina, E. B.; Birshtein, T. M. *Macromolecules* **1995**, *28*, 3562.
(11) Birshtein, T. M.; Zhulina, E. B. *Ber. Bunsen-Ges. Phys. Chem.* **1996**, *100*, 929.
(12) Zhulina, E. B.; Borisov, O. V. *Macromolecules* **1996**, *29*, 2626.
(13) Hariharan, R.; Biver, C.; Russel, W. B. *Macromolecules* **1998**, *31*, 7514.
(14) Borisov, O. V.; Zhulina, E. B. *Eur. Phys. J.* **1998**, *4*, 205.
(15) Klein Wolterink, J.; Leermakers, F. A. M.; Fleer, G. J.; Koopal, L. K.; Zhulina, E. B.; Borisov, O. V. *Macromolecules* **1999**, *32*, 2365.
(16) Zhulina, E. B.; Borisov, O. V.; Birshtein, T. M. *Macromolecules* **1999**, *32*, 8189.
(17) Zhulina, E. B.; Klein Wolterink, J.; Borisov, O. V. *Macromolecules* **2000**, *33*, 4945.
(18) Ahrens, H.; Förster, S.; Helm, C. A. *Macromolecules* **1997**, *30*, 8447.
(19) Ahrens, H.; Förster, S.; Helm, C. A. *Phys. Rev. Lett.* **1998**, *81*, 4172.
(20) An, S. W.; Thirtle, P. N.; Thomas, R. K.; Baines, F. L.; Billingsham, N. C.; Armes, S. P.; Penfold, J. *Macromolecules* **1999**, *32*, 2731.
(21) Currie, E. P. K.; Sieval, A. B.; Avena, M.; Zuilhof, H.; Sudhölter, E. J. R.; Cohen Stuart, M. A. *Langmuir* **1999**, *15*, 7116.
(22) Biesalski, M.; Rühe, J.; Johannsmann, D. *J. Chem. Phys.* **1999**, *111*, 7029.
(23) Tran, Y.; Auroy, P.; Lee, L.-T. *Macromolecules* **1999**, *32*, 8951.
(24) Tran, Y.; Auroy, P. *Eur. Phys. J. E* **2001**, *5*, 65.
(25) Tamashiro, M. N.; Hernandez-Zapata, E.; Schorr, P. A.; Balastre, M.; Tirell, M.; Pincus, P. *J. Chem. Phys.* **2001**, *115*, 1960.
(26) Biesalski, M.; Johannsmann, D.; Rühe, J. *J. Chem. Phys.* **2002**, *117*, 4988.
(27) Biesalski, M.; Johannsmann, D.; Rühe, J. *J. Chem. Phys.* **2004**, *120*, 8807.
(28) Biver, C.; Hariharan, R.; Mays, J.; Russel, W. B. *Macromolecules* **1997**, *30*, 1787.
(29) Hariharan, R.; Biver, C.; Mays, J.; Russel, W. B. *Macromolecules* **1998**, *31*, 7506.
(30) Wesley, R. D.; Cosgrove. T.; Thomson, L.; Armes, S. P.; Billingham, N. C.; Baines, F. L. *Langmuir* **2000**, *16*, 4467.
(31) Moffit, M.; Khougaz, K.; Eisenberg, A. *Acc. Chem. Res.* **1996**, *29*, 95.
(32) Cameron, N. S.; Corbierre, M. K.; Eisenberg, A. *Can. J. Chem.* **1999**, *77*, 1311.
(33) Muller, F.; Delsanti, M.; Auvray, L.; Yang, J.; Chen, Y. J.; Mays, J. W.; Deme, B.; Tirrell, M.; Guenoun, P. *Eur. Phys. J. E* **2000**, *3*, 45.
(34) Muller, F.; Fontaine, P.; Delsanti, M.; Belloni, L.; Yang, J.; Chen, Y. J.; Mays, J. W.; Lesieur, P.; Tirell, M.; Guenoun, P. *Eur. Phys. J. E* **2001**, *6*, 109.
(35) Föster, S.; Hermsdorf, N.; Böttcher, Ch.; Lindner, P. *Macromolecules* **2002**, *35*, 4096.
(36) Groenewegen, W.; Egelhaaf, S. U.; Lapp, A.; van der Maarel, J. R. C. *Macromolecules* **2000**, *33*, 3283.
(37) Groenewegen, W.; Lapp, A.; Egelhaaf, S. U.; van der Maarel, J. R. C. *Macromolecules* **2000**, *33*, 4080.
(38) van der Maarel, J. R. C.; Groenewegen, W.; Egelhaaf, S. U.; Lapp, A. *Langmuir* **2000**, *16*, 7510.
(39) Jusufi, A.; Likos, C. N.; Löwen, H. *Phys. Rev. Lett.* **2002**, *88*, 018301-1.
(40) Jusufi, A.; Likos, C. N.; Löwen, H. *J. Chem. Phys.* **2002**, *116*, 11011.
(41) Manning, G. *Annu. Rev. Phys. Chem.* **1972**, *23*, 117 and further references therein.
(42) See the discussion of this point in: Deserno, M.; Holm, Ch.; Blaul, J.; Ballauff, M.; Rehahn, M. *Eur. Phys. J. E* **2001**, *5*, 97.
(43) Jusufi, A.; Likos, C. N.; Ballauff, M. *Colloid Polym. Sci.* **2004**, *282*, 919.
(44) Guo, X.; Weiss, A.; Ballauff, M. *Macromolecules* **1999**, *32*, 6043.
(45) Guo, X.; Ballauff, M. *Langmuir* **2000**, *16*, 8719.
(46) Guo, X.; Ballauff, M. *Phys. Rev. E* **2001**, *64*, 051406.
(47) de Robillard, Q.; Guo, X.; Ballauff, M.; Narayanan, T. *Macromolecules* **2000**, *33*, 9109.
(48) Das, B.; Guo, X.; Ballauff, M. *Prog. Colloid Polym. Sci.* **2002**, *121*, 34.
(49) Ballauff, M. *Curr. Opin. Colloid Interface Sci.* **2001**, *6*, 132.
(50) Stuhrmann, H. B. *Ad. Polym. Sci.* **1985**, *67*, 123.
(51) Stuhrmann, H. B.; Goerigk, G.; Munk, B. In *Handbook of Synchrotron Radiation*; Ebashi, S., Koch, M., Rubenstein, E., Eds.; Elsevier: Amsterdam, 1991; Vol. 4, Chapter 17, p 557.
(52) Williams, C. *Conf. Proc. Ital. Soc.* **1990**, *25*. Williams, C. In *Neutron, X.-Ray and Light Scattering: Introduction to an Investigative Tool for Colloidal and Polymeric Systems*; Lindner, P., Zemb, Th., Eds.; North Holland: Amsterdam, 1991.
(53) Berg Rasmussen, F.; Molenbroek, A. M.; Clausen, B. S.; Feidenhans, R. *J. Catal.* **2000**, *190*, 205.
(54) Polizzi, S.; Riello, P.; Goerigk, G.; Benedetti, A. *J. Synchrotron Radiat.* **2002**, *9*, 65.
(55) Bota, A.; Goerigk, G.; Drucker, T.; Haubold, H.-G.; Petro, J. *J. Catal.* **2002**, *205*, 354.
(56) Guilleaume, B.; Ballauff, M.; Goerigk, G.; Wittemann, M.; Rehahn, M. *Colloid Polym. Sci.* **2001**, *279*, 829.
(57) Guilleaume, B. Blaul, J.; Ballauff, M.; Wittemann, M.; Rehahn, M.; Goerigk, G. *Eur. Phys. J. E* **2002**, *8*, 299.
(58) Patel, M.; Rosenfeldt, S.; Ballauff, M.; Dingenouts, N.; Pontoni, D.; Narayanan, T. *Phys. Chem. Chem. Phys.* **2004**, *6*, 2962.
(59) Das, R.; Mills, T. T.; Kwok, L. W.; Maskel, G. S.; Millett, I. S.; Doniach, S.; Finkelstein, K. D.; Herschlag, D.; Pollack, L. *Phys. Rev. Lett.* **2003**, *90*, 188103.
(60) Goerigk, G.; Schweins, R.; Huber, K.; Ballauff, M. *Europhys. Lett.* **2004**, *66*, 331.
(61) Dingenouts, N.; Merkle, R.; Guo, X.; Narayanan, T.; Goerigk, G.; Ballauff, M. *J. Appl. Crystallogr.* **2003**, *36*, 578.
(62) Glatter, O., Kratky, O., Eds.; *Small-Angle X-ray Scattering*; Academic Press: London, 1982.
(63) Glikberg, S.; Marcus, Y. *J. Solution Chem.* **1983**, *12*, 255.

(64) Dingenouts, N.; Bolze, J.; Pötschke, D.; Ballauff, M. *Adv. Polym. Sci.* **1999**, *144*, 1.
(65) Henke, B. L.; Gullikson, E. M.; Davis, J. C. *At. Data Nucl. Data Table* **1993**, *54*, 181.
(66) Brennan, S.; Cowan, P. L. *Rev. Sci. Instrum.* **1992**, *63*, 850.
(67) Narayanan, T.; Diat, O.; Boesecke, P. *Nucl. Instrum. Methods Phys. Res. A* **2001**, *467*, 1005.
(68) Beniaminy, I.; Deutsch, M. *Comput. Phys. Commun.* **1980**, *21*, 271.

MA048828J